Received: 18 January 2020 | Revised: 17 March 2020 | Accepted: 15 April 2020

DOI: 10.1002/mrm.28310

FULL PAPER

Magnetic Resonance in Medicine

Improved velocity-selective-inversion arterial spin labeling for cerebral blood flow mapping with 3D acquisition

Dapeng Liu[1,2] | **Feng Xu**[1,2] | **Wenbo Li**[1,2] | **Peter C. van Zijl**[1,2] | **Doris D. Lin**[1] | **Qin Qin**[1,2]

[1]The Russell H. Morgan Department of Radiology and Radiological Science, The Johns Hopkins University School of Medicine, Baltimore, Maryland, USA

[2]F.M. Kirby Research Center for Functional Brain Imaging, Kennedy Krieger Institute, Baltimore, Maryland, USA

Correspondence
Qin Qin, F.M. Kirby Research Center for Functional Brain Imaging, Kennedy Krieger Institute, 707 N. Broadway, Baltimore, MD 21205, USA.
Email: qqin1@jhu.edu

Funding information
National Institute of Biomedical Imaging and Bioengineering, Grant/Award Number: P41 EB015909; American Society of Hematology, Grant/Award Number: Scholar Award; National Heart, Lung, and Blood Institute, Grant/Award Number: K25 HL121192, K25 HL145129, R01 HL135500, R01 HL138182 and R01 HL144751

Purpose: To further optimize the velocity-selective arterial spin labeling (VSASL) sequence utilizing a Fourier-transform based velocity-selective inversion (FT-VSI) pulse train, and to evaluate its utility for 3D mapping of cerebral blood flow (CBF) with a gradient- and spin-echo (GRASE) readout.

Methods: First, numerical simulations and phantom experiments were done to test the susceptibility to eddy currents and B_1 field inhomogeneities for FT-VSI pulse trains with block and composite refocusing pulses. Second, the choices of the post-labeling delay (PLD) for FT-VSI prepared 3D VSASL were evaluated for the sensitivity to perfusion signal. The study was conducted among a young-age and a middle-age group at 3T.

Both signal-to-noise ratio (SNR) and CBF were quantitatively compared with pseudo-continuous ASL (PCASL). The optimized 3D VSI-ASL was also qualitatively compared with PCASL in a whole-brain coverage among two healthy volunteers and a brain tumor patient.

Results: The simulations and phantom test showed that composite refocusing pulses are more robust to both eddy-currents and B_1 field inhomogeneities than block pulses. 3D VSASL images with FT-VSI preparation were acquired over a range of PLDs and PLD = 1.2 s was selected for its higher perfusion signal. FT-VSI labeling produced quantitative CBF maps with 27% higher SNR in gray matter compared to PCASL. 3D whole-brain CBF mapping using VSI-ASL were comparable to the corresponding PCASL results.

Conclusion: FT-VSI with 3D-GRASE readout was successfully implemented and showed higher sensitivity to perfusion signal than PCASL for both young and middle-aged healthy volunteers.

KEYWORDS
3D GRASE acquisition, arterial spin labeling, cerebral blood flow, velocity-selective inversion

1 | INTRODUCTION

Arterial spin labeling (ASL) is attractive for repeated non-invasive monitoring of tissue perfusion. In the recent consensus paper,[1] a standardized protocol using pseudo-continuous arterial spin labeling (PCASL) with a single post-labeling delay (PLD) of 1.8-2 s and 3D acquisition with background suppression,[2] was recommended for quantification of cerebral blood flow (CBF) in clinical applications such as dementia.

Similar to other spatially selective ASL methods which label blood in the feeding arteries at the neck region, CBF could be underestimated if the arterial transit time (ATT) for a certain brain region is longer than the PLD.[3] Techniques have been developed to measure ATT separately as a pre-scan[4] or to estimate CBF and ATT concurrently using multiple PLDs[5-7] or with a Hadamard-encoded scheme.[8,9] However, for patients with compensatory collateral flows in the setting of large-vessel stenosis or occlusion (e.g., Moyamoya), there is conspicuous CBF underestimation (after ATT correction derived from multi-PLD PCASL) for ATT values longer than 4 s.[10] This is related to poor signal-to-noise ratio (SNR) resulting from longitudinal relaxation of labeled blood water when extending PLDs to account for the prolonged ATT.

In addition, the labeling efficiency of PCASL is sensitive to the B_0 field inhomogeneity over the labeling plane, which is distant from the shimming area centered on the imaging volume.[11-13] Parameters for the PCASL labeling pulses were recently optimized to improve their robustness to off-resonance.[14] Furthermore, prescribing labeling planes for PCASL without a survey of individual vascular anatomy around the neck regions can cause variations of labeling efficiency. Placing the labeling plane above the carotid bifurcation and between the second and third vertebrae was found to yield consistent results across subjects.[14] However, this requires additional time for angiography and manual placement for labeling location.

Velocity-selective ASL (VSASL) techniques[15,16] offers advantages over the spatially selective ASL methods in being insensitive to transit time delays and in not needing to prescribe an additional labeling plane. Therefore, VSASL has greater potential for more reproducible clinical application and an easier and faster clinical workflow. However, conventional velocity-selective saturation (VSS) based labeling[15-20] has limited SNR compared to inversion based methods. Recently, Fourier transform based velocity-selective inversion (FT-VSI) pulse train was proposed, indeed demonstrating a higher SNR.[21]

Previous approaches[15-21] have mostly used 2D acquisitions. However, for ASL based CBF mapping, a 3D readout is preferred for larger spatial coverage, more spatially consistent background suppression, higher SNR efficiency, and simpler perfusion quantification. Segmented 3D gradient- and spin-echo (GRASE) acquisition with whole-brain coverage is one of the recommended imaging methods in the standardized ASL protocol for clinical translation.[1] Recently, FT-VSI with low-flip-angle segmented 3D stack-of-spirals and without using background suppression pulses was performed at multiple PLDs to characterize the tracer kinetics of the VSI labeling and used for perfusion-based functional MRI.[22]

The current work aims to optimize FT-VSI with a 3D GRASE readout for baseline perfusion mapping. First, the effect of eddy currents (ECs) with B_1 offset incurred in the brain at 3T was examined with both block and composite refocusing pulses in the FT-VSI label/control pulse trains through numerical simulation and phantom experiments. Second, the optimum PLD for maximizing perfusion signal was evaluated for FT-VSI prepared 3D VSASL. Then, both SNR and CBF were compared between PCASL and FT-VSI VSASL with optimized PLDs. Finally, we demonstrated 3D FT-VSI ASL with whole-brain coverage on two healthy volunteers and a brain tumor patient.

2 | METHODS

2.1 | Kinetic model of VSASL

Following the general kinetic model of pulsed ASL,[23] assuming ATT = 0 and an infinite bolus duration for the ideal case of VSASL, the arterial input function (AIF), a(t), can be described as:

$$a(t) = 2\alpha_{label} \cdot M_{0,blood} \cdot \left(e^{-t/T_{1,blood}}\right). \quad (1)$$

Here t = 0 is defined as the end of the labeling pulse; the factor 2 applies to inversion (specifically, VSI) and would be 1 for saturation (specifically, VSS); α_{label} is the corresponding labeling efficiency; and $M_{0,blood}$ is the equilibrium magnetization of blood.

And the impulse response function (IRF), r(t), is traditionally characterized by both a flow clearance function, $e^{-ft/\lambda}$, and a magnetization relaxation function, $e^{-t/T1,tissue}$:

$$r(t) = e^{-ft/\lambda} \cdot e^{-t/T_{1,tissue}} \quad (2)$$

f is the blood flow (mL/g/s) and λ is the tissue/blood partition coefficient (0.9 ml/g). Note that for a typical CBF of 50 mL/100 g/min or $f = 50/6000$ mL/g/s, f/λ is approximately 1% of $1/T_{1,tissue}$, which is negligible. Equation (2) can thus be simplified as:

$$r(t) = e^{-t/T_{1,tissue}}. \quad (3)$$

The perfusion-weighted ASL signal, as the difference between the control and labeled images, is the convolution between the AIF (Equation (1)) and IRF (Equation (3)):

$$\Delta M(t) = f \cdot a(t) \otimes r(t)$$
$$= 2\alpha_{label} \cdot M_{0,blood} \cdot f \cdot \int_0^t e^{-t'/T_{1,blood}} \cdot e^{-(t-t')/T_{1,tissue}} dt'. \quad (4)$$

Both t and T_1 values are expressed in units of second.

$$\Delta M(t) = 2\alpha_{label} \cdot M_{0,blood} \cdot f \cdot \left(e^{-t/T_{1,blood}} - e^{-t/T_{1,tissue}}\right) / \left(1/T_{1,tissue} - 1/T_{1,blood}\right). \quad (5)$$

Thus, by taking the derivative of Equation (5) to be 0, the time at the maximal perfusion-weighted signal can be determined to be:

$$t_{max} = log\left(T_{1,blood}/T_{1,tissue}\right) / \left(1/T_{1,tissue} - 1/T_{1,blood}\right) \quad (6)$$

which is a value between tissue T_1 and blood T_1.

For the sake of simplicity, the difference in T_1 between blood and tissue is commonly assumed to be small[1,3] and an effective T_1 (1.65 s) is used in the calculation:

$$\Delta M(t) = 2\alpha_{label} \cdot M_{0,blood} \cdot f \cdot t \cdot e^{-t/T_{1,eff}}. \quad (7)$$

Similarly, it is straightforward to obtain the time at the maximal perfusion-weighted signal, when $t_{max} = T_{1,eff}$.

2.2 | Numerical simulation

Numerical simulations using the Bloch equations based on matrix rotation were performed to assess the properties of the FT-VSI pulse trains using Matlab (MathWorks, Inc., Natick, MA, USA). The FT-VSI pulse train, as detailed in,[21] is specified in Supporting Information Figure S1, which is available online. Note that the cut-off velocity for FT-VSI module, 2.8 cm/s, is calculated using the same equation as for the conventional VSS pulse trains,[15] $Vc = \pi/(\gamma m1)$, where γ is the proton gyromagnetic ratio and m1 is the applied first gradient moment. The effect of ECs on the static spins after applying FT-VSI pulse trains with block and composite refocusing pulses ($90°_x 180°_y 90°_x$) were examined. Subtracted responses of the longitudinal magnetizations (Mz) following both the velocity-sensitive label and velocity-compensated control (unipolar gradient lobes) pulse trains were calculated with EC amplitude of 0.025% and time constants of 10^{-4}-1 s for static spins at distances from −23 cm to 24 cm as described by Qin et al,[21,24] with an interval of 0.1 mm. Their sensitivity to various B_1^+ scales, which are the ratio of actual flip angles to nominal input flip angles, from 0.7 to 1.3, were evaluated.

2.3 | Experiments

All experiments were performed on a 3T scanner (Prisma, Siemens Healthineers, Erlangen, Germany) with a 20-channel head/neck receiver coil. Evaluation of both eddy-current and B_1 related effects were conducted on a phantom with both block and composite refocusing pulses. Three in vivo experiments were performed: Exp. 1, Evaluation of multi-delay 3D ASL with FT-VSI preparations to obtain the respective optimal PLDs that yield the maximal perfusion-weighted signal; Exp. 2, Assessment of SNR and CBF quantification between 3D PCASL and VSI-ASL with the optimized PLD; Exp. 3, Demonstration of 3D VSI-ASL with whole-brain coverage.

All volunteers participated in this study after providing informed consent in accordance with the Institutional Review Board guidelines. Ten healthy volunteers were divided into a young-age group (22-31 years old, 3 male and 2 female) and a middle-age group (52-63 years old, 2 male and 3 female) and were recruited for both Exp. 1 and Exp. 2. Two healthy volunteers (a 42-year-old male and a 31-year-old female) and a patient with histopathology-proven glioblastoma (GBM) recurrence (61-year-old, male) were recruited for Exp. 3.

2.4 | Pulse sequences

Pulse sequence diagrams for PCASL and VSI-ASL with 3D acquisition are shown in Figure 1B. It includes five blocks within each repetition: slab-selective saturation, label/control modules using either pseudo-continuous or FT-VSI pulse trains,

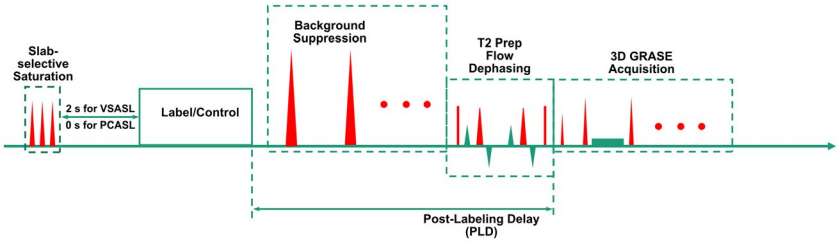

FIGURE 1 Pulse sequence diagram of the ASL sequences used in this study, with FT-VSI or PCASL label/control pulse trains, combined with slab-selective saturation pulses post acquisition, spatially selective BGS pulses during the PLD, and a T_2-prep module with flow-dephasing gradients for suppressing large-vessel signal followed by 3D GRASE acquisition

background suppression, flow-dephasing for suppressing large-vessel signal, and 3D GRASE readout. Spatially selective pre-saturation was a product module with three slab-selective saturation pulses consecutively applied. For VSI-ASL with different PLDs, there was always a 2.0 s delay between the pre-saturation and the labeling modules to allow the inflow of fresh arterial blood into the imaging volume.

The 64-ms labeling and control modules of FT-VSI pulse trains were as described in the Numerical Simulation section. For *in vivo* experiments, all block refocusing pulses were replaced by composite pulses to achieve better insensitivity to B_1 inhomogeneity and less EC artifacts (this is demonstrated in the Results section). Note that the composite pulses ($90°_x180°_y90°_x$) applied in this study doubled the duration of the block pulses and also reduced the gap time between the velocity-encoding gradients and the following RF pulses from 1.32 ms to 0.77 ms, while keeping the total duration of FT-VSI pulse train constant.

Flow-dephasing module was a T2 prepare pulse train (TE_{prep} = 20 ms) comprising ±90° hard pulses and double refocused composite (DRCP) pulses ($90°_x180°_y90°_x$, 1 ms) surrounded by four gradient lobes (6.2 mT/m, 3.6 ms, 0.2 ms ramp time) with cutoff velocity of 2.8 cm/s. Note that this DRCP pulse train could be shortened to reduce T2 decay with eddy-current effect carefully evaluated.

All gradients used in the VSI label/control modules as well as flow-dephasing modules were along the foot-head direction.

Note that FT-VSI pulse trains preserve blood signal in the label modules and invert the magnetization in the control modules so that typically adopted subtraction order, control-label, leads to negative perfusion-weighted signal. For background suppression (BGS), three spatially nonselective inversion pulses were used for VSI-ASL and two inversion pulses for PCASL, in order to have consistent polarity of subtraction results. The timing of the BGS inversion pulses for various PLDs were tailored through a homemade algorithm in Matlab, to minimize the residual signal intensities for static tissue while keeping them consistently positive before acquisition. Since Mz values at the end of VS modules are affected by both T_2 relaxation (as a result of the extended pulse train duration) and B_1 scale due to the use of hard pulses,[25] the effects of T_2, B_1, in addition to T_1 of tissues were taken into account during the optimization of the timing of BGS pulses.

In the calculation, tissue T_1 values ranged from 0.7 to 2.0 s and CSF T_1 from 3.0 to 4.0 s.[26] Tissue T_2 value was assumed to be 80 ms[26] and CSF T_2 was assumed to be 1500 ms.[27] B_1 scales varied from 0.85 to 1.15. Empirically, in order to minimize negative perfusion signal from magnitude subtraction between label and control data, the residual Mz at the end of a PLD was constrained for tissue to be greater than 10% and for CSF to be greater than 0%. The timing of the BGS pulses of all ASL sequences used in this study are listed in Table 1.

TABLE 1 Timing of the BGS pulses for PCASL and FT-VSI ASL sequences used in this study[a]

Methods	PLD (s)	Timing (s) of BGS pulses		
		Pulse 1	Pulse 2	Pulse 3
PCASL	2.00	0.31	1.53	N/A
VSASL (FT-VSI)	0.60	0.27	0.28	0.30
	0.90	0.06	0.09	0.58
	1.20	0.52	0.91	1.08
	1.50	0.65	1.25	1.44
	1.80	0.74	1.47	1.72

[a]The timing is defined as the delay from the end of the labeling module to the center of the BGS pulses.

For all the experiments, the common parameters for the 3D GRASE readout were: excitation flip angle = 90°; refocusing flip angles = 120°; bandwidth = 3004 Hz; acquisition resolution = 3.4 × 3.4 × 4 mm^3, reconstruction resolution = 1.7 × 1.7 × 1.7 mm^3; axial in-plane field of view (FOV) = 220 × 220 mm^2.

An unbalanced PCASL (B_1 of 1.8 μT, average gradient of 0.5 mT/m and maximum gradient of 3.5 mT/m) was implemented following the newly optimized protocol to improve robustness to off-resonance and pulsatile flow velocity.[14]

In addition, a proton density-weighted image (repetition time [TR] = 10.0 s) was acquired to approximate the equilibrium magnetization of tissue ($M_{0,tissue}$) for CBF quantification and a double inversion recovery (DIR) image to visualize gray matter only (TR = 10.0 s; TI_1 = 3.58 s; TI_2 = 0.48 s). All of these images were collected with the same 3D GRASE acquisition scheme as used in the ASL protocols.

2.5 | Phantom experiments

Both block and composite refocusing pulses were tested on a spherical oil phantom by scaling all the pulses in the label/control modules with three different B_1^+ settings, (0.7, 1.0, and 1.3). The PLD was chosen as 1.2 s with corresponding timing of BGS pulses (Table 1). The readout covered 30 slices, of which the first and last three slices were discarded due to fold-over along the slice direction. Fast spin echo (FSE) factor was 10 and echo planar imaging (EPI) factor was 13, with an echo spacing of 11.7 ms. An echo train duration of 117 ms was chosen for low T_2-decay induced blurring and high SNR efficiency.[28] Twelve segments were acquired for each dynamic scan with a partial Fourier transform of 72%. TR was chosen as short

as possible to allow three label/control pairs of dynamics within 4.5 min. Proton density-weighted image of signal intensity (SI_{PD}) was also acquired with TR = 10.0 s.

2.6 | In vivo experiments

For Exp. 1-3, composite refocusing pulses and normal B_1^+ were used. In Exp. 1 (PLD optimization), five PLDs ranging from 0.6 s to 1.8 s in 0.3-s intervals were tested for VSI-ASL. Eight slices covering the middle portion of the brain were acquired. The shimming region was adjusted larger to cover the whole brain. FSE factor was 10 and EPI factor was 23. Two segments were acquired for each dynamic scan. Echo train duration was 165 ms. TR was chosen as short as possible for each PLD to allow 8 label/control pairs within 1.8 min for 0.6 s PLD (TR = 3.0 s), and 2.5 min for 1.8 s PLD (TR = 4.2 s).

For Exp. 2 (PCASL and VSI-ASL comparison), the protocols of VSI-ASL were similar as in Exp. 1, except that the PLD was chosen as 1.2 s (see the Results section) and the number of label/control pairs for averaging was increased to 20 allowing for sufficient SNR. For PCASL, PLD was set as 2.0 s as recommended for clinical use,[1] with 16 averages, so that the acquisition times of both PCASL and VSI-ASL were about 5 min each. The same 3D readout and flow suppression modules were applied for a fair comparison.

For Exp. 3 (whole-brain evaluation both on healthy subjects and a patient), the readout of PCASL and VSI-ASL were similar as in Exp. 1. Keeping their 2.0-s and 1.2-s PLDs as in Exp. 2, this took 5.5 min and 4.5 min to acquire three pairs of repeats for PCASL and VSI-ASL, respectively.

2.7 | Data analysis

Experimental data were processed using Matlab and ImageJ (Rasband W., National Institutes of Health, USA, version 1.51 s).[29] Normalized perfusion signal equal to the averaged subtraction of label/control pairs (ΔS) divided by $S_{0,tissue}$, ($\Delta S/S_{0,tissue}$), was calculated as an indicator of perfusion signal level.

Based on the kinetic model of VSASL (Equation (7)), CBF was quantified as:

$$CBF = 6000 \cdot \lambda \cdot \Delta S/(2\alpha_{label} \cdot \alpha_{BGS} \cdot S_{0,tissue} \cdot e^{-TE_{prep}/T_{2,tissue}} \cdot PLD \cdot e^{-PLD/T_{1,eff}}) \quad (8)$$

where CBF (mL/100 g/min) = 6000 • f (mL/g/s) and $S_{0,tissue}$ is related to $S_{0,blood}$ through the brain-blood partition coefficient, $\lambda = 0.9$ ml/g.[30] Correction factors for signal attenuation due to BGS and tissue T_2 decay during flow-dephasing module were added in Equation (7). The efficiency for BGS (α_{BGS}) was assumed to be 0.95 for each inversion pulse applied[1] and T_2 of gray matter was assumed to be 80 ms. $T_{1,eff}$ was taken as 1.65 s as averaged between T_1 values of gray matter (1.4 s) and blood (1.9 s) at 3T.[31,32] Note that T_1 of white matter is about 0.8 s,[33] and the use of the 1.65 s $T_{1,eff}$ would lead to underestimation of white matter CBF. Labeling efficiency (α_{label}) of VSI-ASL was estimated using the averaged gray matter CBF calculated from PCASL in Exp. 2 across all 10 subjects in both the young- and middle-age groups. For PCASL, Equation (1) in Ref. 1 with $\alpha_{label} = 0.85$ and additional α_{BGS} and $T_{2,tissue}$ decay factors were applied for CBF quantification.

SNR was compared between 3D VSI-ASL and PCASL techniques in Exp. 2 following the steps described in[34] to minimize the effects of both spatially variable noise levels associated with the parallel reconstruction[35] and temporally fluctuated physiologic noise such as cardiac pulsation and respiratory cycles.[36] Briefly, the systematic noise level was assessed as the spatial standard deviation (SD) on the temporal difference images of every two repetitions of control-label subtractions in the image background outside of the head. SNR was then calculated as the mean perfusion-weighted signal within the regions of interest (ROIs) divided by this standard deviation of the background noise.

The gray matter ROIs were generated by applying individually adjusted thresholds on DIR images. Averaged CBF and SNR values from gray matter ROIs were calculated for each ASL method applied in Exp. 2. Student's t-test was performed to test perfusion signal and SNR difference between methods (significance level set at $P = .05$). The correlation of the measured CBF values between the VSI-ASL and PCASL were also analyzed.

3 | RESULTS

3.1 | Numerical simulation

Figure 2 displays the simulated sensitivities of static spins to EC effects for the FT-VSI pulse trains using block and composite refocusing pulses at B_1^+ scales of 0.7, 1.0, and 1.3, respectively. The sensitivities are shown as the subtracted errors of label and control affected by ECs normalized to the equilibrium signal. Note that severe B_1 offsets are known to generate stripe artifacts due to imperfect refocusing, as characterized in previous velocity-selective MR angiography (VSMRA) studies.[37,38] To suppress this periodic banding of high spatial-frequency, the final response Mz was displayed as the average of Mz in 4 mm intervals, to be consistent with the spatial resolution of the ASL experiments. The effect of ECs, which should be zero at the isocenter and increase with the distance to the center, is more severe when B_1^+ offset is present and mostly within the range of time constants of 10-3-10-1 s. Notably, a baseline artifact primarily associated with B_1^+ offset is

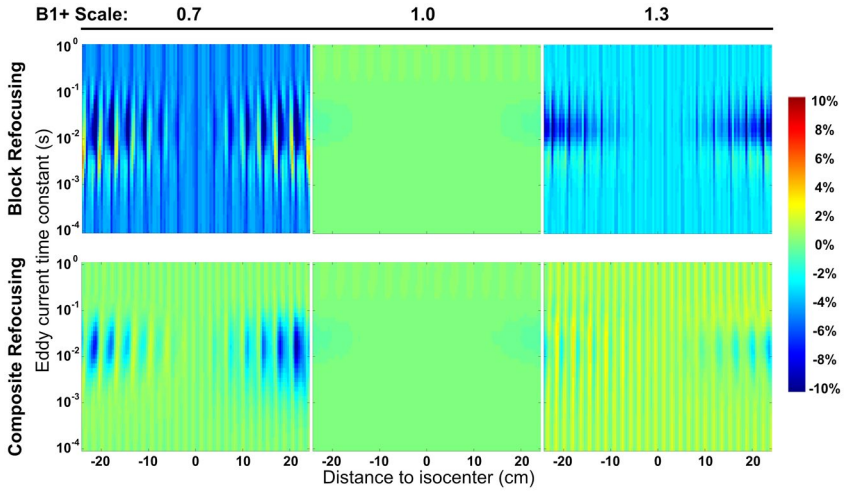

FIGURE 2 Simulated subtraction errors of static spins following a FT-VSI pulse train applying block (first row) and composite (second row) refocusing pulses, with EC effects of different time constants at varying distances to isocenter at B_1^+ scales of 0.7 (left column), 1.0 (middle column), and 1.3 (right column). Large errors from incorrect B_1^+ settings were reduced substantially when switching from block to composite refocusing pulses

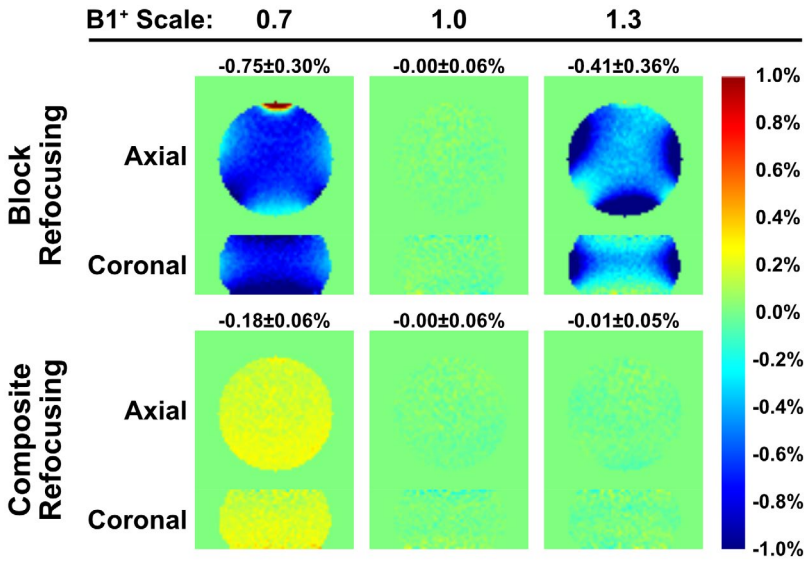

FIGURE 3 Normalized subtracted signal of the phantom experiment using FT-VSI based VSASL with PLD of 1.2 s and 3D GRASE acquisition. In the VSI pulse trains, block (first row) and composite (second row) refocusing pulses were applied, at B_1^+ scales of 0.7 (left column), 1.0 (middle column), and 1.3 (right column). Incorrect B_1^+ settings yielded considerable false signal for block refocusing pulses, which were reduced substantially when using composite refocusing pulses, similar to the findings of numerical simulation results in Figure 2

also observed, which is not dependent on either the spatial distance or the time constants of ECs. When setting the amplitude of the ECs to zero, this B_1 related artifact does not change (data not shown). Compared to block refocusing pulses (Figure 2, first row), composite refocusing pulses (Figure 2, second row) reduce both EC and B_1 related errors considerably for B_1^+ scales both lower (= 0.7, Figure 2, left column) and higher (= 1.3, Figure 2, right column) than correct settings (= 1.0, Figure 2, middle column). This robustness to B_1 inhomogeneity prompted the adoption of the composite refocusing pulses for FT-VSI pulse trains applied in the following in vivo experiments.

3.2 | Phantom experiments

Normalized subtracted signal, defined as (label-control)/M_0, are displayed in Figure 3. The pattern of the false signal from the phantom experiments is close to the simulation results (Figure 2), with both EC related effects at the edge of the phantom and B_1 related errors spatially independent. For block refocusing pulses (Figure 3, first row), artifactual signal were substantially higher under ±30% B_1 offset than under correct B_1 setting, and were largely suppressed when using composite refocusing (Figure 3, second row). The subtraction errors (mean ± SD) averaged across all 24 slices of the phantom for block and composite refocusing pulses are −0.75 ± 0.30% vs. −0.18 ± 0.06% at $B_1^+ = 0.7$, and −0.41 ± 0.36% vs. −0.01 ± 0.05% at $B_1^+ = 1.3$, respectively. It is worth mentioning that the stripe artifact due to B_1 imperfection was tangled with the EC effect and is under investigation currently.

3.3 | In vivo experiments

For Exp. 1 of the PLD optimization, representative data of one participant from the young-age group and one from the middle-age group are displayed in Figure 4A,B, respectively.

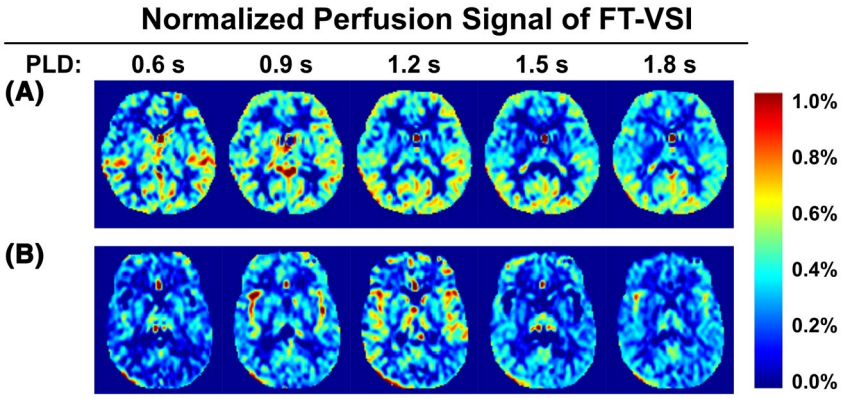

FIGURE 4 Normalized perfusion signal images using FT-VSI preparations acquired with PLDs from 0.6 s to 1.8 s with examples (one slice) from one female subject (31 yo) of the young-age group (A) and one male subject (52 yo) of the middle-age group (B)

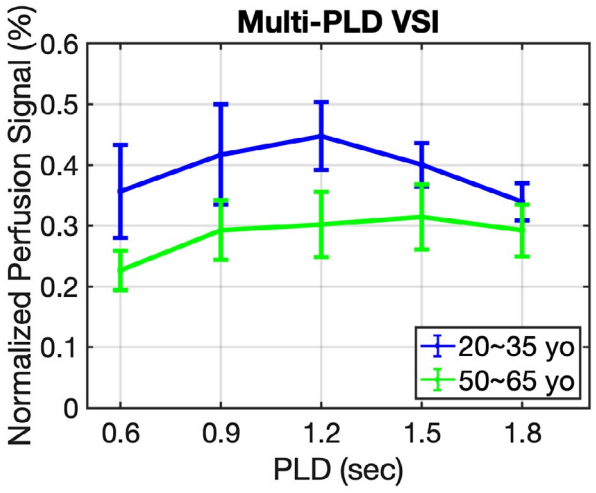

FIGURE 5 Normalized perfusion signal in gray matter using FT-VSI preparations as function of PLD averaged across the young-age group (blue) and the middle-aged group (green)

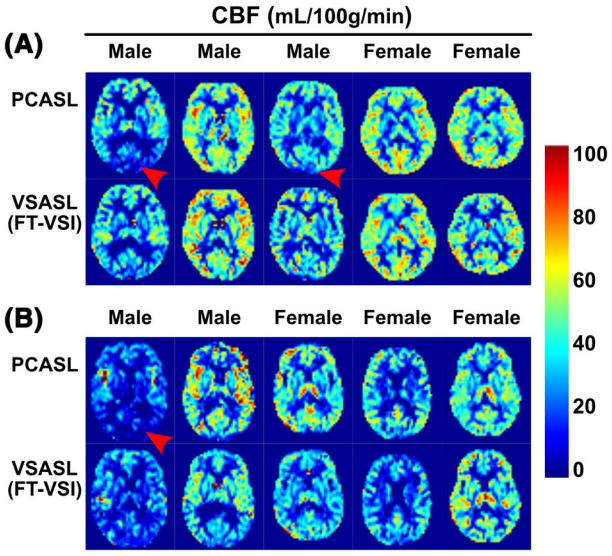

FIGURE 6 Quantitative CBF maps (one slice) using PCASL and FT-VSI prepared VSASL of each participant from the young-age group (A) and the middle-age group (B). Note that the PCASL results of several subjects show CBF underestimation in the occipital lobes (red arrowhead), most likely related to its sensitivity to long transit time delay or inefficient labeling. In contrast, VSASL results do not display such artifacts

The normalized perfusion-weighted images ($\Delta S/S_{0,tissue}$) from VSI-ASL with 3D GRASE acquisition at five different PLDs from 0.6 s to 1.8 s are shown (only one middle slice as an example). The perfusion-weighted images at various PLDs display rather uniform contrast through different regions of the brain as expected from its ATT-insensitive nature. When averaged in gray matter across subjects, the normalized perfusion signal (Figure 5) was plotted as a function of PLDs for the groups of young-age (blue) and the middle-age (green). For all subjects, the perfusion signal levels of VSI-ASL techniques are low at 0.6 s PLD, increase to a peak around 1.2 s and 1.5 s and then, become lower at PLD = 1.8 s. Young-age group had ~13% higher perfusion signal at 1.2 s PLD than at 1.5 s and no significant difference was found between the two PLDs for middle-aged group. Considering that shorter PLD requires shorter TR and, hence, a better temporal resolution, PLD of 1.2 s was chosen as the optimized PLD for the subsequent VSI-ASL scans. At PLD of 1.2 s, middle-aged participants exhibit lower perfusion signal in comparison with the younger subjects for VSI-ASL results ($P = .001$).

In Exp. 2, quantitative 3D CBF maps were derived using PCASL (PLD = 2.0 s) as well as FT-VSI based VSASL scans (PLD = 1.2 s) in ten healthy volunteers, respectively. By referencing with PCASL derived mean gray matter CBF across these subjects, the labeling efficiency of FT-VSI was estimated to be $\alpha_{label} = 0.61$. The CBF maps calculated using PCASL and VSI-ASL are arrayed for all the subjects of the young-age (Figure 6A) and middle-age (Figure 6B) groups (only one middle slice shown). Visually both ASL techniques showed comparable perfusion results in cortical areas as well as deep brain regions. Compared to VSI-ASL results, the PCASL based CBF maps of several male subjects show artifactually low CBF in the occipital lobes (Figure 6, red arrowheads).

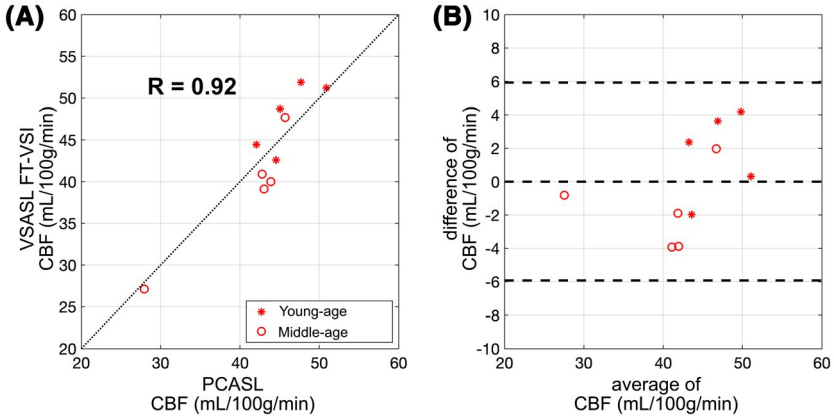

FIGURE 7 Correlation (A) and agreement (B) plots of the averaged individual CBF values measured between FT-VSI prepared VSASL and PCASL of gray matter ROIs from subjects of the young (stars) and the middle-age (open circles) groups. For the correlation plots (A), the black dashed lines show the unity line y = x. The Bland-Altman plot are shown in (B), in which the difference of the two methods are plotted against their mean, with the middle of the three horizontal dashed lines indicating the mean difference of all subjects, and the top and bottom dashed lines indicating the mean difference ± two times of the standard deviation of their differences

TABLE 2 Averaged CBF and spatial SNR values in gray matter ROIs of two different ASL methods for both the young and middle-aged groups (mean ± SD, $N = 5$), respectively

		CBF (mL/100 g/min)	SNR
PCASL	Young-age	46.3 ± 3.0	16.5 ± 2.2
	Middle-age	40.7 ± 7.2	14.3 ± 3.8
VSASL (FT-VSI)	Young-age	48.3 ± 3.9	21.5 ± 3.6
	Middle-age	39.2 ± 7.5	17.6 ± 4.7

Figure 7 shows correlation and Bland-Altman analyses of the averaged individual CBF values from both gray matter comparing FT-VSI prepared VSASL with PCASL. Overall, there is excellent consistency between PCASL and VSI-ASL for CBF quantification with a correlation coefficient of 0.92.

Averaged CBF and SNR values within gray matter ROIs are reported in Table 2 for PCASL and VSI-ASL of both the young- and middle-aged groups. Both VSASL and PCASL results show that middle-age subjects have 12-19% lower gray matter CBF than young-age ones ($P < .001$). Averaged across both age groups, the SNR value of FT-VSI in gray matter (19.6 ± 4.5) is 27% higher than that of PCASL (15.4 ± 3.1) ($P < .001$).

Figure 8 shows the whole-brain CBF mapping results of Exp. 3 using PCASL and FT-VSI prepared VSASL of two healthy volunteers (Figure 8A,B) and a patient with recurrent left occipital GBM (Figure 8C). The perfusion signal in frontal lobe, temporal lobe, parietal lobe, occipital lobe, and cerebellum are consistent between PCASL and VSI-ASL, and their contrast between gray matter and white matter correspond well with the gray matter-only images by DIR. A hyperperfused region in the tumor of the patient with recurrent GBM is well depicted by both ASL methods (Figure 8, red arrowheads).

4 | DISCUSSION

VSASL has the advantage of insensitivity to transit time delay compared to the spatially selective method, thus potentially providing more accurate and robust blood flow measurements in cerebrovascular diseases. Furthermore, the VSI scheme could naturally have better SNR than conventional VSS scheme. The present study optimized FT-VSI labeled VSASL using the 3D GRASE acquisition and evaluated the CBF quantitation and SNR estimation by comparing with PCASL sequences at 3T among both young and middle-aged healthy volunteers. A number of technical challenges were addressed, and some require additional considerations.

A previous VSMRA study has explored the use of composite refocusing pulses within the velocity-selective pulse trains.[25] In that paper, block pulses were recommended over composite pulses for refocusing, due to the adequate immunity of Mz-velocity response to B_0/B_1 field inhomogeneities with shorter pulse durations and less SAR constraints. For VSASL, when only correct B_1^+ scales were evaluated with respect to gradient imperfections, block refocusing pulses were shown sufficient to suppress false signal from static tissue.[21,24] In this current work, when poor B_1 conditions were examined as large spatial coverage would incur, simulations of Mz-position responses (Figure 2), as well as phantom (Figure 3) and human (Supporting Information Figure S2) results all demonstrated that composite refocusing pulses were more robust over block refocusing to minimize both eddy-current and B_1 related artifacts. The erroneous phases from eddy-currents associated with gradient lobes surrounding the refocusing

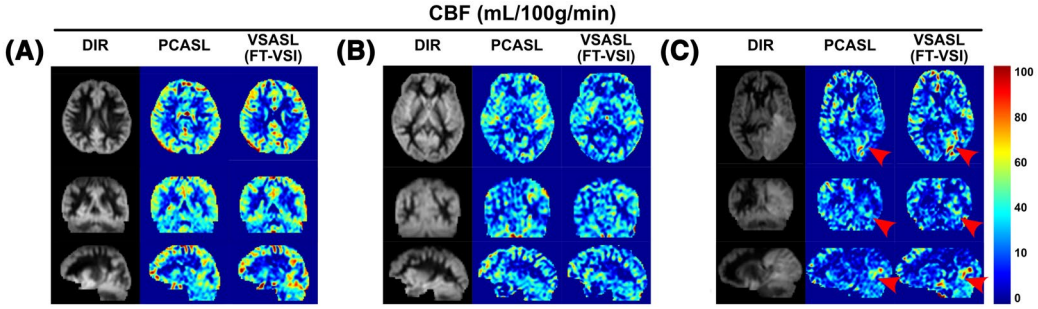

FIGURE 8 CBF maps of PCASL and FT-VSI based VSASL along axial, sagittal and coronal views of a female subject (31 yo) (A), a male subject (42 yo) (B), and a male patient (61 yo) with recurrent glioblastoma in the left occipital lobe (C, red arrowhead). The perfusion signal across brain regions are consistent between PCASL and VSI-ASL, and their contrast closely resemble the gray-matter-only anatomical images by DIR

pulses might be better canceled, when B_1 is with correct setting (middle column of Figures 2 and 3), or refocusing pulses are less sensitive to B_1 offset (second row of Figures 2 and 3).

For 3D acquisition with FT-VSI labeling, the design of the timing of BGS pulses is critical. Tissue inversion by the FT-VSI pulse train needs to be included in the BGS calculation. Since the duration of FT-VSI pulse train (64 ms) is close to gray matter T_2 (70-100 ms),[26] T_2 relaxation during the labeling was also calculated. The inversion degree of the FT-VSI pulse train is also sensitive to the B_1 field inhomogeneity, as a result of applying nine of 20° block pulses at the beginning of each velocity-encoding step.[21,39] Applying magnitude subtraction resulted in a negative perfusion signal when T_2 and B_1 effects were not considered (data not shown). Particularly, accounting for a range of B_1^+ scales and ensuring all residual Mz at the end of BGS to be positive yielded non-uniform suppression of background signal intensity with a range of 2-10%. Subtraction with complex data and phase correction[40] could allow more uniform BGS for VSASL and is currently under investigation.

It is worth mentioning that, in addition to VSI, another possible method to improve SNR efficiency is using multiple VSS modules in VSASL.[41] Perfusion sensitivity of FT-VSI prepared VSASL might be further enhanced by applying repeated labeling modules.[41,42] Although both VSS and VSI are velocity-selective based, there is slight difference in principle, as the former assumes laminar flow. Nonetheless, using multi-PLD measurements, the ATT values for gray matter were estimated to be close to zero for both VSS[41] and FT-VSI based VSASL.[22]

The PLD optimization for 3D VSASL images with FT-VSI preparation concluded a good PLD to be 1.2-1.5 s (Figures 3 and 4), which is consistent with the finding of earlier works.[17,22,41] Note that 1.2 s is a little shorter than the predicted value from the theoretical kinetic model (Equation (5)), which is between T_1 of gray matter (1.20-1.40 s) and blood (1.70-1.90 s) at 3T,[31,43,44] or the effective T_1 (1.65 s) taken in the simplified model (Equation (7)). This might reflect practical issues related to velocity-selective labeling. The arterial input function (Equation (1)) assumes that the labeling efficiency is uniform through the bolus duration. However, the trailing edge of the arterial bolus, mainly the blood in the neck region or the heart, is expected to have lower labeling efficiency as a result of blood velocity, transmit coil coverage and B_0/B_1 inhomogeneity, thus could shorten the peak time of the kinetic curve. Furthermore, the measured signal might contain unwanted contributions from blood vessels related to the choice of the cut-off velocity and the gradient direction, which could also shift the peak time earlier.[17] With this regard, 1.5 s PLD is desired to mitigate the inflow effect and allow labeled spins into the tissue, especially for elderly subjects with slower flow velocities. In this work, 2.8 cm/s were chosen as the cut-off velocity for both FT-VSI labeling and flow-dephasing module, applied along the foot-head direction. Blood spins flowing perpendicular to the fixed direction would not be properly labeled or dephased, and direction looping or segment encoding might provide alternative schemes to mitigate the direction dependence of VSASL.[17]

The factors that individually affect the labeling efficiency of FT-VSI based VSASL include: B_0/B_1 field inhomogeneity, temporal variation of velocity during the pulse, T_2 relaxation, vessel orientation, and velocity-compensated configuration for the control module. In this study with 3D acquisition, the labeling efficiency was estimated using mean gray matter CBF across all subjects measured by PCASL as reference, which is rather consistent with our earlier study using conventional VSS with 2D acquisition as reference,[21] 0.61 vs. 0.57. Although this artificially makes the group-averaged CBF values derived from PCASL and VSI-ASL to be the same, the excellent correlation across young- and middle-age subjects (Figure 7) demonstrates high individual agreement between the two methods.

FT-VSI labeling produced quantitative CBF maps with about 27% higher SNR in gray matter compared to PCASL for both young and middle-aged healthy volunteers (Table 2). In contrast, as recorded in the earlier study,[21] FT-VSI yielded 9% lower SNR than PCASL. This difference is likely due to a change from four BGS pulses applied previously for PCASL

to two pulses in the current study, which led to a less optimal suppression of background noise. Another factor contributing to this discrepancy could be associated with the 1.2 s PLD chosen in this study vs. 1.5 s used before. Younger subjects with faster inflow were shown to have higher perfusion signal at 1.2 s PLD than at 1.5 s (Figure 5). The 12-19% lower gray matter CBF measured among middle-age subjects compared to the young cohort is in concordance with the previously reported change across three or four decades with a decrement in CBF of 0.38% per year.[45] White matter CBF values were not quantified in this study due to the low perfusion signal, as well as the quantification errors related to both the misrepresented $T_{1,eff}$ as mentioned in Data Analysis and the nonzero ATT for white matter estimated by FT-VSI based ASL with multiple PLDs.[22] The lower CBF in the posterior regions estimated by PCASL (red arrowhead in Figure 6) indicated that a long arterial transit delay may cause underestimated perfusion using PCASL, even with a PLD as long as 2.0 s. Similar observation on healthy subjects using pulsed ASL has also been reported previously,[20] showing the intrinsic disadvantage of spatially selective ASL techniques. Alternatively, this could also be attributed to inefficient labeling for PCASL in the arteries supplying these regions due to slow blood velocity or vessel tortuosity, which could be verified by MRA.

The CBF mapping with 3D whole-brain coverage among several subjects including a patient demonstrates the potential of 3D FT-VSI based VSASL for clinical applications. Validations in various clinical settings are warranted before wider adoption of this relatively new ASL approach.

5 | CONCLUSIONS

A FT-VSI ASL sequence with optimized pulse train configuration and PLD with 3D GRASE acquisition was successfully implemented. The sequence demonstrated higher sensitivity to perfusion signal than PCASL. FT-VSI based VSASL with 3D whole-brain coverage may further enhance ASL's clinical applicability by maximizing its sensitivity to perfusion signal with minimum susceptibility to transit time delay, systematic errors and background noise.

ORCID

Dapeng Liu https://orcid.org/0000-0002-4432-3202
Wenbo Li https://orcid.org/0000-0002-0199-1534
Qin Qin https://orcid.org/0000-0002-6432-2944

REFERENCES

1. Alsop DC, Detre JA, Golay X, et al. Recommended implementation of arterial spin-labeled perfusion MRI for clinical applications: A consensus of the ISMRM perfusion study group and the European consortium for ASL in dementia. *Magn Reson Med*. 2015;73:102-116.
2. Ye FQ, Frank JA, Weinberger DR, McLaughlin AC. Noise reduction in 3D perfusion imaging by attenuating the static signal in arterial spin tagging (ASSIST). *Magn Reson Med*. 2000;44:92-100.
3. Alsop DC, Detre JA. Reduced transit-time sensitivity in noninvasive magnetic resonance imaging of human cerebral blood flow. *J Cereb Blood Flow Metab*. 1996;16:1236-1249.
4. Dai W, Robson PM, Shankaranarayanan A, Alsop DC. Reduced resolution transit delay prescan for quantitative continuous arterial spin labeling perfusion imaging. *Magn Reson Med*. 2012;67:1252-1265.
5. MacIntosh BJ, Filippini N, Chappell MA, Woolrich MW, Mackay CE, Jezzard P. Assessment of arterial arrival times derived from multiple inversion time pulsed arterial spin labeling MRI. *Magn Reson Med*. 2010;63:641-647.
6. Wang DJJ, Alger JR, Qiao JX, et al. Multi-delay multi-parametric arterial spin-labeled perfusion MRI in acute ischemic stroke – Comparison with dynamic susceptibility contrast enhanced perfusion imaging. *NeuroImage Clin*. 2013;3:1-7.
7. Qin Q, Huang AJ, Hua J, Desmond JE, Stevens RD, van Zijl PCM. Three-dimensional whole-brain perfusion quantification using pseudo-continuous arterial spin labeling MRI at multiple post-labeling delays: Accounting for both arterial transit time and impulse response function. *NMR Biomed*. 2014;27:116-128.
8. Dai W, Shankaranarayanan A, Alsop DC. Volumetric measurement of perfusion and arterial transit delay using hadamard encoded continuous arterial spin labeling. *Magn Reson Med*. 2013;69:1014-1022.
9. Teeuwisse WM, Schmid S, Ghariq E, Veer IM, van Osch MJP. Time-encoded pseudocontinuous arterial spin labeling: Basic properties and timing strategies for human applications. *Magn Reson Med*. 2014;72:1712-1722.
10. Fan AP, Guo J, Khalighi MM, et al. Long-delay arterial spin labeling provides more accurate cerebral blood flow measurements in Moyamoya patients: A simultaneous positron emission tomography/MRI study. *Stroke*. 2017;48:2441-2449.
11. Jahanian H, Noll DC, Hernandez-Garcia L. B0 field inhomogeneity considerations in pseudo-continuous arterial spin labeling (pCASL): Effects on tagging efficiency and correction strategy. *NMR Biomed*. 2011;24:1202-1209.
12. Jung Y, Wong EC, Liu TT. Multiphase pseudocontinuous arterial spin labeling (MP-PCASL) for robust quantification of cerebral blood flow. *Magn Reson Med*. 2010;64:799-810.
13. Chen Z, Zhang X, Yuan C, Zhao X, van Osch MJP. Measuring the labeling efficiency of pseudocontinuous arterial spin labeling. *Magn Reson Med*. 2017;77:1841-1852.
14. Zhao L, Vidorreta M, Soman S, Detre JA, Alsop DC. Improving the robustness of pseudo-continuous arterial spin labeling to off-resonance and pulsatile flow velocity. *Magn Reson Med*. 2017;78:1342-1351.
15. Wong EC, Cronin M, Wu WC, Inglis B, Frank LR, Liu TT. Velocity-selective arterial spin labeling. *Magn Reson Med*. 2006;55:1334-1341.
16. Duhamel G, de Bazelaire C, Alsop DC. Evaluation of systematic quantification errors in velocity-selective arterial spin labeling of the brain. *Magn Reson Med*. 2003;50:145-153.
17. Wu WC, Wong EC. Intravascular effect in velocity-selective arterial spin labeling: The choice of inflow time and cutoff velocity. *NeuroImage*. 2006;32:122-128.
18. Qiu D, Straka M, Zun Z, Bammer R, Moseley ME, Zaharchuk G. CBF measurements using multidelay pseudocontinuous and

velocity-selective arterial spin labeling in patients with long arterial transit delays: Comparison with xenon CT CBF. *J Magn Reson Imaging*. 2012;36:110-119.
19. Meakin JA, Jezzard P. An optimized velocity selective arterial spin labeling module with reduced eddy current sensitivity for improved perfusion quantification. *Magn Reson Med*. 2013;69:832-838.
20. Guo J, Meakin JA, Jezzard P, Wong EC. An optimized design to reduce eddy current sensitivity in velocity-selective arterial spin labeling using symmetric BIR-8 pulses. *Magn Reson Med*. 2015;73:1085-1094.
21. Qin Q, van Zijl PCM. Velocity-selective-inversion prepared arterial spin labeling. *Magn Reson Med*. 2016;76:1136-1148.
22. Hernandez-Garcia L, Nielsen JF, Noll DC. Improved sensitivity and temporal resolution in perfusion FMRI using velocity selective inversion ASL. *Magn Reson Med*. 2019;81:1004-1015.
23. Buxton RB, Frank LR, Wong EC, Siewert B, Warach S, Edelman RR. A general kinetic model for quantitative perfusion imaging with arterial spin labeling. *Magn Reson Med*. 1998;40:383-396.
24. Qin Q, Qu Y, Li W, et al. Cerebral blood volume mapping using Fourier-transform-based velocity-selective saturation pulse trains. *Magn Reson Med*. 2019;81:3544-3554.
25. Qin Q, Shin T, Schär M, Guo H, Chen H, Qiao Y. Velocity-selective magnetization-prepared non-contrast-enhanced cerebral MR angiography at 3 Tesla: Improved immunity to B0/B1 inhomogeneity. *Magn Reson Med*. 2016;75:1232-1241.
26. Stanisz GJ, Odrobina EE, Pun J, et al. T1, T2 relaxation and magnetization transfer in tissue at 3T. *Magn Reson Med*. 2005;54:507-512.
27. Qin Q. A simple approach for three-dimensional mapping of baseline cerebrospinal fluid volume fraction. *Magn Reson Med*. 2011;65:385-391.
28. Qin Q. Point spread functions of the T2 decay in k-space trajectories with long echo train. *Magn Reson Imaging*. 2012;30:1134-1142.
29. Schneider CA, Rasband WS, Eliceiri KW. NIH image to imageJ: 25 years of image analysis. *Nat Methods*. 2012;9:671-675.
30. Herscovitch P, Raichle ME. What is the correct value for the brain–blood partition coefficient for water? *J Cereb Blood Flow Metab*. 1985;5:65-69.
31. Qin Q, Strouse JJ, van Zijl PCM. Fast measurement of blood T1 in the human jugular vein at 3 Tesla. *Magn Reson Med*. 2011;65:1297-1304.
32. Li W, Grgac K, Huang A, Yadav N, Qin Q, van Zijl PCM. Quantitative theory for the longitudinal relaxation time of blood water. *Magn Reson Med*. 2016;76:270-281.
33. Lu H, Nagae-Poetscher LM, Golay X, Lin D, Pomper M, van Zijl PCM. Routine clinical brain MRI sequences for use at 3.0 Tesla. *J Magn Reson Imaging*. 2005;22:13-22.
34. Zhao L, Chang CD, Alsop DC. Controlling T2 blurring in 3D RARE arterial spin labeling acquisition through optimal combination of variable flip angles and k-space filtering. *Magn Reson Med*. 2018;80:1391-1401.
35. Dietrich O, Raya JG, Reeder SB, Reiser MF, Schoenberg SO. Measurement of signal-to-noise ratios in MR images: Influence of multichannel coils, parallel imaging, and reconstruction filters. *J Magn Reson Imaging*. 2007;26:375-385.
36. Zhao L, Alsop DC, Detre JA, Dai W. Global fluctuations of cerebral blood flow indicate a global brain network independent of systemic factors. *J Cereb Blood Flow Metab*. 2019;39:302–312.
37. Shin T, Qin Q, Park JY, Crawford RS, Rajagopalan S. Identification and reduction of image artifacts in non–contrast-enhanced velocity-selective peripheral angiography at 3T. *Magn Reson Med*. 2016;76:466-477.
38. Shin T, Qin Q. Characterization and suppression of stripe artifact in velocity-selective magnetization-prepared unenhanced MR angiography. *Magn Reson Med*. 2018;80:1997-2005.
39. Li W, Xu F, Schär M, et al. Whole-brain arteriography and venography: Using improved velocity-selective saturation pulse trains. *Magn Reson Med*. 2017;79:2014-2023.
40. Maleki N, Dai W, Alsop DC. Optimization of background suppression for arterial spin labeling perfusion imaging. *Magn Reson Mater Physics, Biol Med*. 2012;25:127-133.
41. Guo J, Wong EC. Increased SNR efficiency in velocity selective arterial spin labeling using multiple velocity selective saturation modules (mm-VSASL). *Magn Reson Med*. 2015;74:694-705.
42. Xu J, Qin Q, Wu D, et al. Steady pulsed imaging and labeling scheme for noninvasive perfusion imaging. *Magn Reson Med*. 2016;75:238-248.
43. Wu W-C, Jain V, Li C, et al. In vivo venous blood T1 measurement using inversion recovery true-FISP in children and adults. *Magn Reson Med*. 2010;64:1140-1147.
44. Varela M, Hajnal JV, Petersen ET, Golay X, Merchant N, Larkman DJ. A method for rapid in vivo measurement of blood T1. *NMR Biomed*. 2011;24:80-88.
45. Chen JJ, Rosas HD, Salat DH. Age-associated reductions in cerebral blood flow are independent from regional atrophy. *NeuroImage*. 2011;55:468-478.

SUPPORTING INFORMATION

Additional Supporting Information may be found online in the Supporting Information section.

FIGURE S1 The sequence diagram of the 64 ms FT-VSI pulse train: it is composed of nine excitation pulses (20° hard pulses) with eight velocity-encoding steps, with each step (8 ms) interleaved with paired and phase-cycled refocusing pulses and four triangular gradient lobes with alternating polarity (21.8 mT/m, 0.6 ms duration, 0.3 ms ramp time, 2.8 cm/s cut-off velocity). The duration of block (180°y) and composite (90°x180°y90°x) refocusing pulses are 0.5 and 1.0 ms, with post-gaps following gradient lobes of 1.02 and 0.77 ms, respectively

FIGURE S2 Quantitative CBF maps (one slice) derived from FT-VSI prepared VSASL applying block (first row) and composite (second row) refocusing pulses on a young male subject (left column) and a middle-aged female subject (right column). Abnormal perfusion signal can be observed in the anterior brain regions (marked by red arrows) for block refocusing pulses but is suppressed when composite refocusing pules were used. This is consistent with the eddy-current effect under poor B_1 offset as demonstrated in the numerical simulation results (Figure 2) and phantom results (Figure 3)

How to cite this article: Liu D, Xu F, Li W, van Zijl PC, Lin DD, Qin Q. Improved velocity-selective-inversion arterial spin labeling for cerebral blood flow mapping with 3D acquisition. *Magn Reson Med*. 2020;84:2512–2522. https://doi.org/10.1002/mrm.28310